Teaching RoboClam to Dig: The Design, Testing, and Genetic Algorithm Optimization of a Biomimetic Robot

Amos G. Winter, V, Robin L. H. Deits, Daniel S. Dorsch, Anette E. Hosoi,
and Alexander H. Slocum, *Member, IEEE*

***Abstract*— Razor clams (*Ensis directus*) are one of nature's most adept burrowing organisms, able to dig to 70cm at nearly 1cm/s using only 0.21J/cm. We discovered that *Ensis* reduces burrowing drag by using motions of its shell to fluidize a thin layer of substrate around its body. We have developed RoboClam, a robot that digs using the same mechanisms as *Ensis*, to explore how localized fluidization burrowing can be extended to engineering applications. In this work we present burrowing performance results of RoboClam in *Ensis'* habitat. Using a genetic algorithm to optimize RoboClam's kinematics, the machine was able to burrow at speeds comparable to *Ensis*, with a power law relationship between digging energy and depth of n = 1.17, close to the n = 1 achieved by the animal. Pushing through static soil has a theoretical energy-depth power law of n = 2, which means that *Ensis*-inspired digging motions can provide exponential energetic savings over existing burrowing methods.**

I. Introduction

THE motivation behind this work is to generate compact, lightweight, low-energy, reversible, and dynamic burrowing systems for use in subsea applications such as anchoring, oil recovery, mine detonation, and sensor placement. As many organisms have evolved to embed themselves into undersea substrates [1-11], our hypothesis is that nature has found an optimized solution to subsea burrowing. We identified the Atlantic razor clam, *Ensis direcuts,* as the best candidate for biomimicry because of its performance and engineering merits. *Ensis* burrows at nearly 1cm/s to 70cm deep using approximately 0.21J/cm [2, 9-11], which equates to being able to travel over a half kilometer on the energy in a AA battery [12]. Furthermore, razor clams are the size scale of a real engineering device (3.2cm diameter, 16cm long), and are packaged in a rigid shell with only one degree-of-freedom movement. Using the animal's performance and geometry, we have calculated that an *Ensis*-based burrowing/anchoring system would provide a 10X improvement over the best currently available anchoring technology, leading most by more than two orders of magnitude, in anchoring force developed per unit energy expended [13-15].

The burrowing cycle of a razor clam is shown in Fig. 1a-f. b) The animal starts with its foot - a soft, flexible organ - fully extended below the shell. Next, it uses a series of four shell motions to make downward progress: c) the foot extends to uplift the shell; d) the shell halves contract to force blood into the foot, inflating it to serve as an anchor; e) the foot muscles contract to pull the shell downwards; and f) the shell expands in order to begin the cycle again. To understand the soil mechanics during this cycle, we developed an experimental setup to visualize a razor clam burrowing in 1mm soda lime glass beads, which are similar in size and density to coarse sand [16]. A video of *Ensis* burrowing in our setup can be seen here [17]. Substrate deformation was tracked using particle image velocimetry (PIV) [18]. We discovered that the uplift and contraction movements of the shell draw water towards the animal's body, unpacking and locally fluidizing the surrounding substrate, as shown in Fig. 1g.

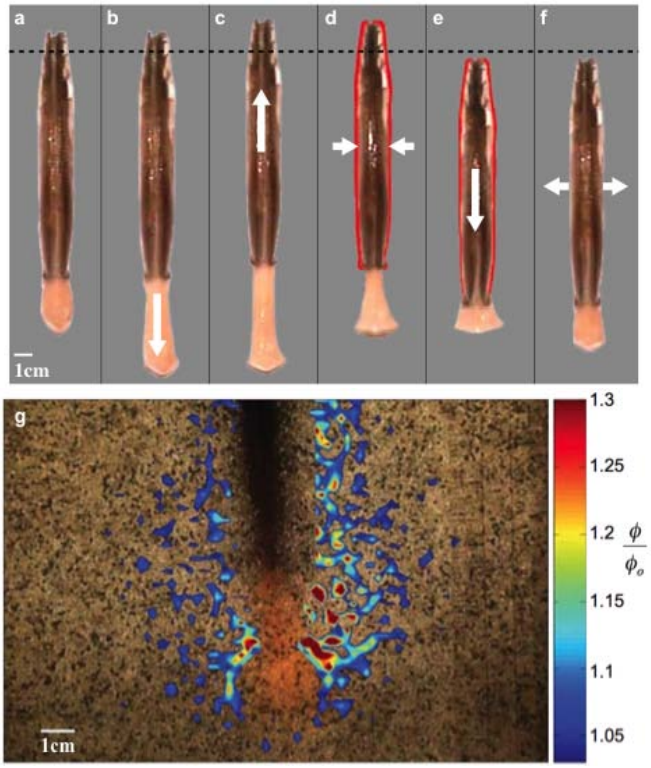

Fig. 1. Razor clam burrowing motions and localized fluidization. a-f) Razor clam digging kinematics. g) Localized fluidization generated during uplift and contraction shell motion. Colored regions denote fluidization, as measured by particle image velocimetry, plotted as current void fraction (ϕ) divided by initial void fraction (ϕ_o).

Manuscript received March 10, 2010. This work was supported by the Battelle Memorial Institute, Bluefin Robotics, and the Chevron Corporation.

All authors are with the Department of Mechanical Engineering at the Massachusetts Institute of Technology.

A. E. Hosoi is the author of correspondence, 77 Massachusetts Ave., Room 3-262, Cambridge, MA 02139 USA; phone: (617) 253-4337; email: peko@mit.edu.

Moving through fluidized, rather than packed soil, reduces the amount of energy *Ensis* has to expend to reach full burrow depth by an order of magnitude when compared to a blunt body the same size and shape, as shown by Fig. 2. Furthermore, because *Ensis* moves through a fluidized medium, the drag force on its body should ideally remain constant with depth. In contrast, moving through a packed, static particulate medium, as in the case of the blunt body, requires pushing force that increases linearly with depth [19]. This means *Ensis* exponentially reduces burrowing energy from scaling with depth squared to linearly increasing with depth, even though some energy is required to locally fluidize the soil.

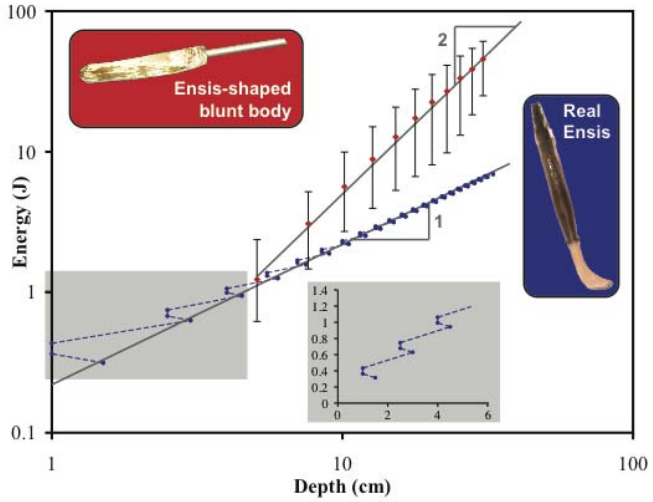

Fig. 2. Burrowing energetics of *Ensis* and a blunt body the same size and shape as the animal. Blunt body data acquired during 15 tests in *Ensis* habitat off the coast of Gloucester, MA. Ensis data adapted from [9]. Ensis achieves an exponential reduction in burrowing energy by moving through locally fluidized, rather than packed soil.

II. Experimental Design

A. RoboClam Design

To verify that localized fluidization drag reduction could be transferred to engineering burrowing applications, we developed RoboClam, a robot that replicates *Ensis* digging kinematics. RoboClam was designed to yield insight into the relationships between environmental and engineering parameters, such as substrate type, depth, device size, burrowing velocity, and required power. Figure 3a shows the end effector of RoboClam – the part of the robot that digs by mimicking *Ensis* shell motions to locally fluidize surrounding substrate – during its burrowing cycle. In RoboClam, *Ensis'* foot has been replaced by a pneumatic piston that pushes down on the end effector, as we have found from our experiments that only *Ensis'* shell motions contribute to localized fluidization.

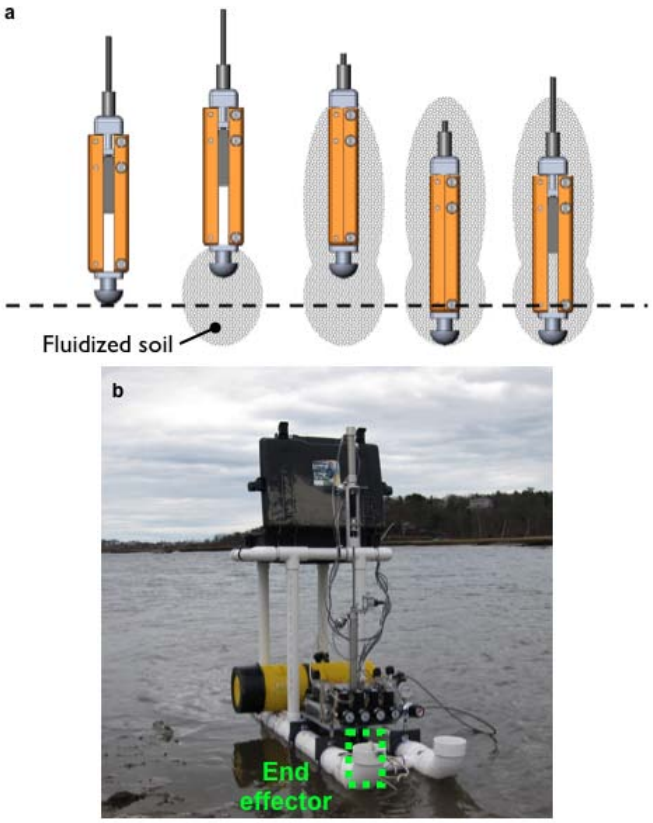

Fig. 3. RoboClam. a) End effector mechanism, which moves with kinematics similar to razor clam burrowing to locally fluidize surrounding substrate. b) RoboClam burrowing in a mud flat off the coast of Gloucester, MA. Location of end effector relative to robot outlined in green. When burrowing, the end effector is covered by a neoprene boot to prevent soil from jamming the mechanism.

A requirement of RoboClam was that it could be tested in real marine substrates, as to avoid wall effects caused by a container, and to capture the peculiarities of real soil with heterogeneous composition and the presence of organic matter. Figure 3b shows RoboClam burrowing in real *Ensis* habitat off Gloucester, MA. For saltwater compatibility, RoboClam's main power source is an 80 ft^3 scuba tank. Small lead acid batteries power four solenoid valves and digital pressure regulators that direct air to two pneumatic pistons, which control the end effector's two degrees of freedom. A laptop controls the robot using a genetic algorithm, which is discussed in the following subsection.

The end effector moves in two degrees of freedom: up/down and in/out. The in/out motion is accomplished with a sliding wedge between the two "shells" of the end effector, as shown in Fig. 4a. This mechanism is exactly constrained and has contact lengths/widths greater than two, as to prohibit jamming during any part of the stroke [20]. Furthermore, the wedge intersects the center of pressure on the shell regardless of its position. This prevents the shell from exerting moments on the wedge that could increase frictional losses. The rod used to actuate in/out movement is housed within the rod to move the end effector up and down, providing a compact coupling to RoboClam's actuation and measurement systems. The end effector is surrounded by a

neoprene boot to prevent soil particles from entering the mechanism.

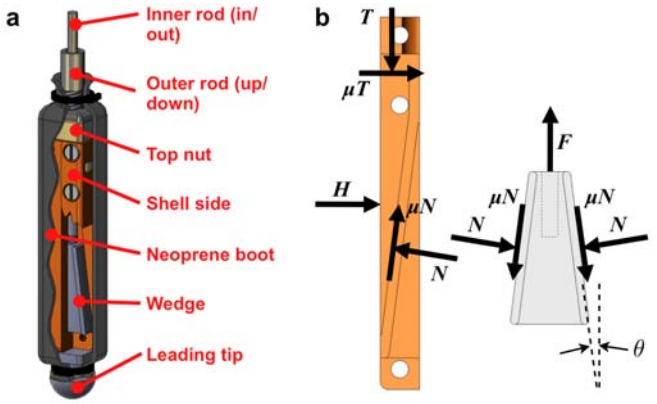

Fig. 4. RoboClam's end effector. a) Functional parts of the end effector and packaging to prevent soil from entering the mechanism. b) Free body diagram of the end effector during expansion/contraction.

The end effector is made from alloy 932 (SAE 660) bearing bronze and 440C stainless steel. These materials were chosen because both are saltwater compatible and have a low coefficient of sliding friction when lubricated [21]. The dynamic coefficient of friction within the mechanism was measured to be 0.173 with 0.013 standard deviation, under horizontal loads ranging from 13.34N to 83.74N. Silicon oil was used as a lubricant because it is not absorbed by the neoprene boot.

The transmission ratio (*TR*) for the mechanism, given in Eq. 1, can be derived from the free body diagram in Fig. 4b

$$TR = \frac{H}{F} = \frac{1}{2}\left[\frac{\cos\theta - \mu\sin\theta}{\sin\theta + \mu\cos\theta} - \mu\right] \tag{1}$$

where F and H are the input and output forces, respectively, θ is the wedge angle, and μ is the measured coefficient of friction. The efficiency of the mechanism, given in Eq. 2, can be calculated by computing the work done over a stroke

$$\eta = \frac{E_{in}}{E_{out}} = 2\frac{H\delta_x}{F\delta_y} = 2TR\sin\theta \tag{2}$$

where E is energy and δ represents the displacements corresponding to the input and output forces.

To determine whether *Ensis*-inspired digging provides and advantage over other methods, the energy expended in soil deformation while burrowing must be calculated. RoboClam's end effector efficiency was measured to be 39% with a minimum of 33% and a maximum of 46%, corresponding to 6σ friction measurements. Because this efficiency can be characterized, the energy expended deforming soil while burrowing can be deterministically calculated. This is important, as overall energy consumed is device dependent; we are interested in finding a new burrowing *method* that is more efficient than current methods. After this method is identified, machines used to exploit it can be designed for optimized efficiency.

Soil deformation energy, E_{soil}, can be calculated by accounting for input energy, E_{in}, from the pneumatic pistons, minus losses in the system from friction in the mechanical elements, $E_{friction}$, and changes in potential energy, $E_{potential}$. For the up/down motion of RoboClam, the energy lost to soil deformation during one stroke is

$$\begin{aligned} E_{soil} &= E_{in} - E_{friction} - E_{potential} \\ &= \int_{\delta_1}^{\delta_2} \Delta p_u A_u dy - \left|F_{u,friction}(\delta_2 - \delta_1)\right| \\ &\quad - m_u g(\delta_2 - \delta_1) \end{aligned} \tag{3}$$

where the subscript u designates the up/down piston, Δp_u is the pressure difference over the piston, δ_1 and δ_2 are the starting and ending displacements of the stroke, A_u is the area of the piston, $F_{u,friction}$ is the measured frictional force in the piston, and m_u is the total mass moving up and down.

The energy transferred to the soil during the in/out motion is represented by

$$\begin{aligned} E_{soil} &= \eta(E_{in} - E_{friction} - E_{potential}) - E_{boot} \\ &= \eta\left[\int_{\delta_1}^{\delta_2} \Delta p_i A_i dy - \left|F_{i,friction}(\delta_2 - \delta_1)\right|\right. \\ &\quad \left. - m_i g(\delta_2 - \delta_1)\right] \end{aligned} \tag{4}$$

where the subscript i represents the in/out piston, δ_1 and δ_2 are the starting and ending displacements of the stroke, η is the efficiency defined in Eq. 2, Δp_i is the pressure difference over the piston, A_i is the area of the piston, $F_{i,friction}$ is the measured frictional force in the piston, and m_i is the total mass moving up and down. Energy lost to deformation of the neoprene boot surrounding the end effector, E_{boot}, proved very difficult to measure. Since most of this energy results from elastic deflection of boot, it was taken to be zero over a full in/out cycle. This is a conservative assumption, as any energy lost to hysteresis caused by the viscoelasticity of the neoprene will appear as additional energy dissipated in the soil.

B. Genetic algorithm design

In testing RoboClam, the sequence of the machine's motions (up stroke, contraction, down stroke, expansion) was never varied. The space of control parameters was reduced to the pneumatic force applied for each movement, as well as the duration or displacement of each movement. We experimentally found that time control of the upward and downward motion and displacement control of the inward and outward motions resulted in successful burrowing. This yielded eight independently-controllable parameters: upward and downward time, inward and

outward displacement, and upward, downward, inward, and outward pressure.

We determined that the best optimization strategy for the robot's control parameters was a genetic algorithm (GA), as it could efficiently explore a large cost space in multiple dimensions and enable the RoboClam to *learn* how to dig most efficiently. The random mutation and recombination of traits used by a GA also tend to allow it to find a global minimum, even in situations in which other optimization methods would not [22]. MATLAB's GA was chosen for RoboClam testing, with a population of 10-20 individuals running for 10-20 generations. With the algorithm in direct control of the robot, the GA was able to generate parameters, run the RoboClam, collect data, and analyze the cost for each test, which in turn allowed for extensive testing of a variety of parameters.

In quantifying optimized burrowing performance, two factors proved to be relevant: the overall energy expenditure per depth of the robot, β, and the power law relationship, n, between depth and energy expended. Minimizing only β resulted in low-energy burrowing for depths of 20-30cm, but with relatively high n (>2); at greater depths these burrowing techniques would be useless, as required energy would exponentially increase. As a result, we used the product of β and n for the GA cost, as given in Eq. 5, with the intent of minimizing n to 1 and β as small as possible.

$$GA_{cost} = \beta n \tag{5}$$

III. Experimentation, Results, and Discussion

Figures 5 and 6 show burrowing performance results from RoboClam testing in real razor clam habitat – a mud flat off the coast of Gloucester, MA. The results were obtained from 125 separate trials using parameters generated by the GA. For each test, the robot dug into virgin soil. After the test, the robot was dragged ~6in down the shore to a new spot of virgin soil.

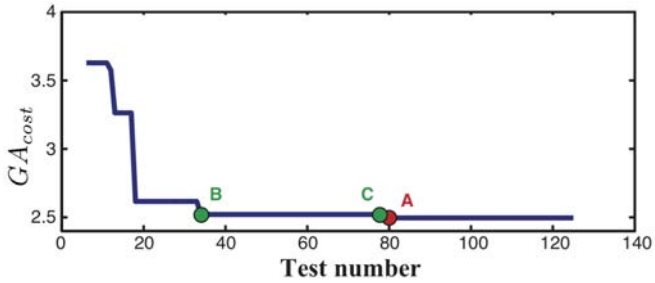

Fig. 5. GA cost results from 125 trials of RoboClam burrowing in a Gloucester, MA mud flat. Each data point corresponds to the lowest cost achieved within the entire trial set, thus far, at each specific trail. Point A is the lowest cost trial measured (2.50 at test 80), in which RoboClam pushed straight into the soil, not using *Ensis* digging motions. Point B is the second lowest cost trial (2.52 at test 34), in which RoboClam did use *Ensis* digging motions. Results from this trial are shown in Fig. 6. Point C is the third lowest cost trial (2.59 at test 78), also in which RoboClam used *Ensis* digging motions.

Figure 5 shows the lowest cost achieved within the entire trial set, thus far, at each specific trail. As can be seen from the figure, the GA successfully minimized the cost over the entire trial set, reaching an asymptote near GA_{cost} = 2.5. The lowest cost measured, at trial 80 and shown at point A in Fig. 5, resulted from RoboClam pushing straight into the soil without using *Ensis* burrowing kinematics. This trail was not considered "best," as the robot did not actually "dig". Additionally, because penetration energy scales with depth squared in static soil, the GA_{cost} associated with this trail would much larger at greater depths.

The trial with the second lowest cost, shown by point B in Fig. 5, was obtained using *Ensis* burrowing kinematics. The associated digging parameters were: up stroke: 0.0854s at 8.96kPa, contraction: 0.0057m at 288kPa, down stroke: 2s at 352kPa, expansion: 0.0057m at 388kPa. Figure 6 shows the burrowing performance corresponding to this trial.

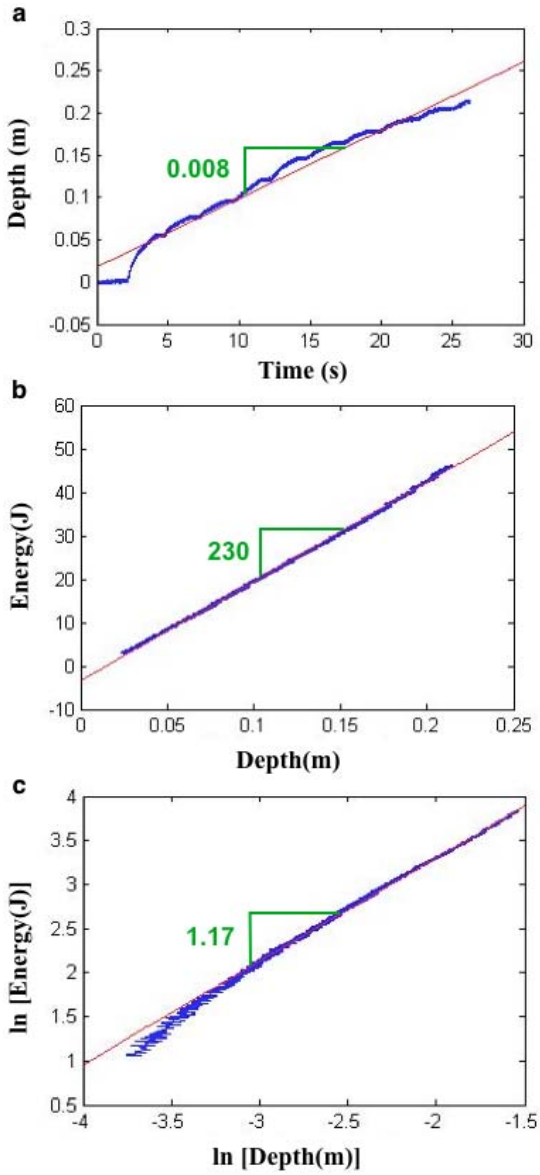

Fig. 6. The second lowest cost mud flat trial, in which the robot used *Ensis* digging motions, corresponding to point B in Fig. 5. a) Burrowing velocity. b) Burrowing energy vs depth. c) Burrowing energy vs depth power law relationship.

In the second lowest cost trial, RoboClam was able to dig at 0.8cm/s, approximately the same speed as *Ensis*, as shown in Fig. 6a. Animal and machine differed in the amount of energy required to burrow (calculated in both cases by determining mechanical energy expended to the soil); Fig. 6b shows that RoboClam required 230J/m, whereas *Ensis* expends only about 21J/m.

Our proposed explanation for this discrepancy is that both animal and machine must operate on similar timescales and velocities (*Ensis'* peak downward stroke velocity is 10cm/s[9], RoboClam's is 2-8cm/s), yet RoboClam has an order of magnitude more mass to move (2.5kg) than *Ensis* (~0.2kg). As a result, the excess kinetic energy in the machine during its downward stroke, which is >10X that of *Ensis*, must get dissipated, presumably in the packed soil below the locally fluidized zone. *Ensis*, with its low mass, can control its movements and only move within the fluidized zone. Thus, our explanation of the energetic discrepancy between animal and machine is due to excess kinetic energy that must be dissipated upon RoboClam's impact with static soil.

Figure 6c shows that RoboClam was able to dig with an energy-depth power law relationship of $n = 1.17$. This result constitutes an enormous energetic savings over simply pushing through static soil (which theoretically has $n = 2$), and is close to the ideal value predicted for *Ensis* of $n = 1$.

IV. Conclusions and Future Work

We have shown that RoboClam is able to achieve exponential burrowing energy reductions over simply pushing through soil. The practical significance of this result is that *Ensis*-inspired devices may be able to dig deeper using less energy than devices that do not take advantage of localized fluidization. The measured energy-depth power law relationship of $n = 1.17$ is close to the ideal value of $n = 1$ predicted for real *Ensis*. Repeated variation of the control parameters and selection for the smallest product of n and β by the GA resulted in a nearly linear force/displacement relationship. Our assumption is that localized fluidization around RoboClam's end effector, as observed during *Ensis* burrowing, is the cause of the measured energetic reductions.

We continue to test RoboClam in various substrates using different size end effectors in order to further understand the limits of *Ensis*-inspired digging. Our aim is to understand the parametric relationships between different substrates, depths, and kinematic configurations. Concurrently with experimentation, we are developing theoretical soil/fluid constitutive models to describe the fluidized region of substrate around a contracting body, as well as the drag associated with moving through the substrate. Empirical and theoretical results will be combined to form design rules to enable engineers to deterministically design burrowing devices for any size scale, substrate type, and performance requirements.

Acknowledgment

The authors would like to thank Mario Bollini and Caitrin Jones for their assistance in testing the RoboClam.

References

[1] Fager, E.W., *Marine Sediments: Effects of a Tube-Building Polychaete*. Science, 1964. **143**(3604): p. 356-359.

[2] Holland, A.F. and J.M. Dean, *Biology of Stout Razor Clam Tagelus-Plebeius .1. Animal-Sediment Relationships, Feeding Mechanism, and Community Biology*. Chesapeake Science, 1977. **18**(1): p. 58-66.

[3] Aoyama, J., et al., *First observations of the burrows of Anguilla japonica*. Journal of Fish Biology, 2005. **67**(6): p. 1534-1543.

[4] Kelly, M.D., et al., *Burrow extension by crack propagation*. Nature, 2005. **433**(7025): p. 475.

[5] Rosenberg, R. and K. Ringdahl, *Quantification of biogenic 3-D structures in marine sediments*. Journal of Experimental Marine Biology and Ecology, 2005. **326**(1): p. 67-76.

[6] Shin, P.K.S., A.W.M. Ng, and R.Y.H. Cheung, *Burrowing responses of the short-neck clam Ruditapes philippinarum to sediment contaminants*. Marine Pollution Bulletin, 2002. **45**(1-12): p. 133-139.

[7] Stanley, S.M., *Bivalve Mollusk Burrowing Aided by Discordant Shell Ornamentation*. Science, 1969. **166**(3905): p. 634-635.

[8] Trueman, E.R., *Bivalve Mollusks: Fluid Dynamics of Burrowing*. Science, 1966. **152**(3721): p. 523-525.

[9] Trueman, E.R., *The Dynamics of Burrowing in Ensis (Bivalvia)*. Proceedings of the Royal Society of London. Series B, Biological Sciences, 1967. **166**(1005): p. 459-476.

[10] Trueman, E.R., *The locomotion of soft-bodied animals*. 1975, London: Edward Arnold.

[11] Trueman, E.R., A.R. Brand, and P. Davis, *The Dynamics of Burrowing of Some Common Littoral Bivalves*. J Exp Biol, 1966. **44**(3): p. 469-492.

[12] Energizer. *Energizer E91 AA Battery Product Datasheet*. 2009. http://data.energizer.com/PDFs/E91.pdf.

[13] Hinz, E.R., *The complete book of anchoring and mooring*. 1 ed. 1986, Centreville, Md: Cornell Maritime Press.

[14] McCormick, M.E., *Anchoring systems*. 1 ed. 1979, New York: Pergamon Press.

[15] Chance, A.B., *Design Methodology: Chance Helical Anchor/Pile Bearing Capacity*. 2006, Hubbell Power Systems.

[16] Lambe, T.W. and R.V. Whitman, *Soil Mechanics*. 1969, New York: John Wiley & Sons.

[17] Winter, A., *Video of burrowing Ensis*. 2008. http://techtv.mit.edu/videos/1334-roboclam

[18] Sveen, J.K., *MatPIV*. 2004. http://folk.uio.no/jks/matpiv/

[19] 19. Robertson, P.K. and R.G. Campanella, *Interpretation of cone penetration tests. Part I: Sand*. Canadian Geotechnical Journal, 1983: p. 718-733.

[20] Slocum, A.H., *Precision machine design*. 1992, Englewood Cliffs, N.J: Prentice Hall.

[21] Avallone, E.A. and I. T. Baumeister, *Marks' Standard Handbook for Mechanical Engineers*. 10 ed. 1996, New York: McGraw-Hill.

[22] RL Haupt, S.H., *Practical Genetic Algorithms*. 2004, Hoboken, NJ: John Wiley & Sons, Inc.